Performance Analysis of Cyclostationary Interference Suppression for Multiuser Wired Communication Systems

Gi-Hong Im and Hui-Chul Won

Abstract: **This paper discusses cyclostationary interference suppression for multiuser wired communication systems. Crosstalk interference from digital signals in multipair cables has been shown to be cyclostationary. Many crosstalk equalization or suppression techniques have been proposed which make implicit use of the cyclostationarity of the crosstalk interferer. In this paper, the convergence and steady-state behaviors of a fractionally spaced equalizer (FSE) in the presence of multiple cyclostationary crosstalk interference are thoroughly analyzed by using the equalizer's eigenstructure. The eigenvalues with multiple cyclostationary interference depend upon the folded signal and interferer power spectra, the cross power spectrum between the signal and the interferer, and the cross power spectrum between the interferers, which results in significantly different initial convergence and steady-state behaviors as compared to the stationary noise case. The performance of the equalizer varies depending on the relative clock phase of the symbol clocks used by the signal and multiple interferers. Measured characteristics as well as analytical model of NEXT/FEXT channel are used to compute the optimum and worst relative clock phases among the signal and multiple interferers.**

Index Terms: **Fractionally-spaced equalizer, interference suppression and cancellation, multiple cyclostationary interference, xDSL and high-speed LAN environments.**

I. INTRODUCTION

Numerous wired and wireless communication channels can be modeled as multi-input multi-output networks, where the received signal suffers from intersymbol interference (ISI), cochannel interference, and additive noise [1]. These multiuser applications include wideband CDMA system, broadband data transmission for digital subscriber line (DSL) [2]–[4] and high-speed local area network (LAN) [5], and high-density digital magnetic recording.

In this paper, we consider multiuser wired communication system for high-speed LAN and DSL applications. High-speed bandwidth-efficient transceivers have been designed for the existing telephone loop plant. Unlike conventional voice-band modems, these transceivers use the full available bandwidth of the copper cables. With the availability of high-speed digital processing technology and the usage of bandwidth-efficient modulation schemes, such as discrete multitone (DMT) [3] and carrierless amplitude and phase modulation (CAP) [5], [6], we can now transmit very high-speed digital data over the existing nonloaded copper loop plant. There are many different versions of DSL systems such as DSL, high-rate DSL (HDSL) [2], asymmetric DSL (ADSL) [3], [6], [7], rate-adaptive DSL (RADSL), and very high-speed DSL (VDSL) [3], [8]–[11], which are being deployed or under field trial by the telephone operators. The telecommunications wiring system that is used in commercial buildings is called a premises distribution system (PDS). Recently, high-speed LAN transmission techniques have been developed to provide duplex operation over copper wiring in PDS system at data rates ranging from 51 Mb/s up to 1 Gb/s [5]. The main signal processing techniques involved in these applications are channel equalization and echo or near-end crosstalk (NEXT) cancellation. The impairments that high-speed digital services must deal with on the copper wiring are well summarized in [2]. For high-speed LAN and xDSL applications, the two major causes of performance degradation for transceivers operating over copper cables are propagation loss and crosstalk generated between adjacent wire pairs, such as NEXT and far-end crosstalk (FEXT). For example, for asynchronous transfer mode (ATM)-LAN and HDSL, which use the same frequency band for both directions, NEXT is the major impairment, whereas for VDSL, which uses different frequency bands for each direction, FEXT is the major impairment [12]. In [13], researchers have pointed out the cyclostationary nature of these crosstalk interferers. Many crosstalk equalization techniques have been proposed which make implicit use of the cyclostationarity of the crosstalk interferer. It has been found that these cyclostationary crosstalks can be suppressed by using transmitter pulse bandwidths which are wide relative to the symbol rate of the signal [5], [14]–[19]. For the special case when the input data sequences generating crosstalks are known at the central office, NEXT cancellers have been proposed [20], similar to data-driven echo cancellers [21], [22].

This paper generalizes the crosstalk equalization or suppression of a single cyclostationary interference [5], [9], [18], [19] to multiuser environment, where multiple cyclostationary crosstalk interferers exist. The equalizer structure assumed for the analysis is a fractionally spaced linear equalizer (FSE) operating over short range loops. Various decision feedback equalizer structures and their performances over longer loop applications such as HDSL and ADSL can be found in [23]. Expressions for the eigenvalues and the minimum mean square error (MMSE) with multiple cyclostationary interference are obtained by using the folded signal and interferer power spectra, the cross power spectrum between the signal and the interferer, and the cross power spectrum between the interferers. We then thoroughly analyze the convergence and steady-state behaviors of a fractionally spaced equalizer (FSE) in the presence of multiple cyclostationary crosstalk interference by using the equalizer's eigen-

Manuscript received January 25, 2003; approved for publication by Yong Hoon Lee, Division I Editor, November 6, 2003.

The authors are with the Communications Research Lab., Pohang Univ. of Science and Technology (POSTECH), Pohang, South Korea, email: igh@postech.ac.kr.

This work was supported in part by grant No.R01-2003-000-11627-0 from the Basic Research Program of the Korea Science & Engineering Foundation.

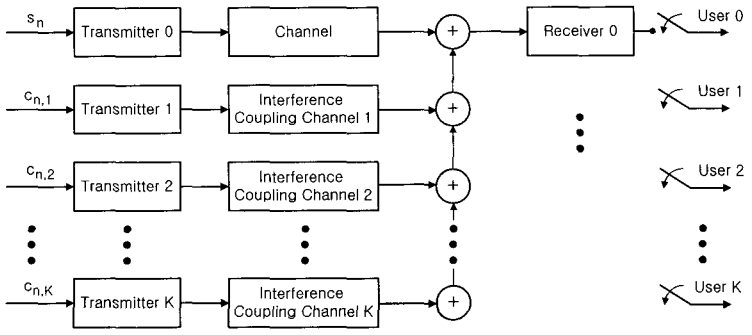

Fig. 1. Multiuser communication system.

structure. It is shown that this peculiar equalizer's eigenstructure in the presence of cyclostationary interference results in significantly different initial convergence and steady-state behaviors as compared to the stationary noise case. It is also shown that the performance of the equalizer varies depending on the relative clock phase of the symbol clocks used by the signal and multiple interferers. Measured characteristics as well as analytical model of NEXT/FEXT channel are used to compute the optimum and worst relative clock phases among the signal and multiple interferers.

This paper is organized as follows. In Section II, the equalizer's eigenstructure in the presence of multiple cyclostationary interference is analyzed, and its excess MSE and MMSE are obtained by using the eigenstructure. In Section III, the performance of cyclostationary interference suppression for multiuser wired communication system is investigated by using the theoretical analysis as well as computer simulations. Finally, we conclude the paper in Section IV.

II. ANALYSIS OF CONVERGENCE AND STEADY-STATE BEHAVIORS IN THE PRESENCE OF MULTIPLE CYCLOSTATIONARY INTERFERENCE

The cyclostationary crosstalk suppression or equalization techniques require that the signals have 100% excess bandwidth per crosstalk interferer [5], [15]–[19]. In other words, a necessary condition for perfect suppression of K interferers in Fig. 1 is that the signal uses an excess bandwidth of at least $K \times 100\%$. Fig. 2(a) shows the most popular shaping filter for bandwidth-efficient digital transmission, which is the so-called raised-cosine family. The transfer function of raised-cosine filter with excess bandwidth smaller than 100% is well known [24], and is expressed as

$$G(f) = \begin{cases} T \quad \text{if} \quad 0 \le |\text{f}| \le \frac{1}{2\text{T}}(1-\alpha) \\ \frac{T}{2} - \frac{T}{2}\sin\frac{\pi T}{\alpha}(|f| - \frac{1}{2T}) \\ \quad \text{if} \quad \frac{1}{2\text{T}}(1-\alpha) \le |\text{f}| \le \frac{1}{2\text{T}}(1+\alpha), \end{cases} \tag{1}$$

where T and α denote the symbol interval and excess bandwidth, respectively. However, when the excess bandwidth is larger than 100%, these expressions are no longer valid and

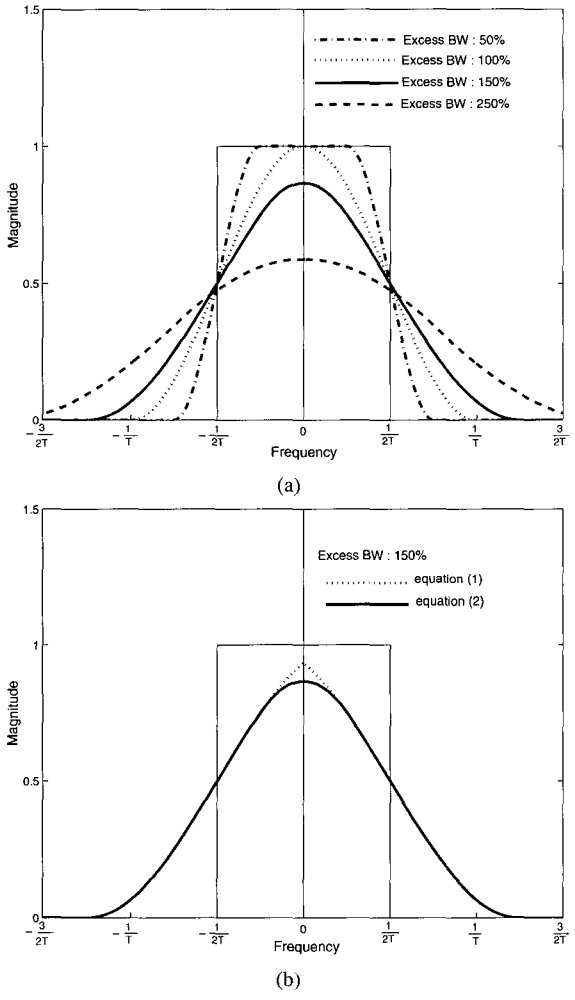

Fig. 2. (a) Transfer function of raised-cosine shaping filter. (b) transfer function with 150% excess bandwidth.

should be modified as

$$G(f) = \begin{cases} -\frac{T}{2}\sin\frac{\pi T}{\alpha}(f - \frac{1}{2T}) + \frac{T}{2}\sin\frac{\pi T}{\alpha}(f + \frac{1}{2T}) \\ \quad \text{if} \quad 0 \le |\text{f}| \le \frac{1}{2\text{T}}(\alpha - 1) \\ \frac{T}{2} - \frac{T}{2}\sin\frac{\pi T}{\alpha}(|f| - \frac{1}{2T}) \\ \quad \text{if} \quad \frac{1}{2\text{T}}(\alpha - 1) \le |\text{f}| \le \frac{1}{2\text{T}}(\alpha + 1). \end{cases} \tag{2}$$

Fig. 2(b) shows two transfer functions of (1) and (2), for 150% excess bandwidth ($\alpha = 1.5$). Notice from Fig. 2(b) that the two curves show different characteristics for $0 \le |f| \le \frac{1}{2T}(\alpha - 1)$. After symbol-rate sampling, the solid line of (2) yields constant folded spectrum, thus satisfying the Nyquist criterion. In this section, we analyze the convergence behavior and steady-state performance of the equalizer when transmitter pulse shaping with large excess bandwidth is used to suppress multiple cyclostationary interferers. The eigenstructure of the equalizer in the presence of multiple cyclostationary interference is first analyzed, and then the equalizer's convergence behavior and steady-state performance are investigated by using its eigenvalues.

A. Eigenvalues and Eigenvectors

The real received signal at the input of the receiver of 'user 0' in Fig. 1 can be expressed as

$$r(t) = \mathrm{Re}\left[\sum_{n=-\infty}^{\infty} s_n h(t-nT) + \sum_{l=1}^{K}\sum_{n=-\infty}^{\infty} c_{n,l}x_l(t-nT-\theta_l T')\right], \quad \theta_l = 0,1,\cdots,2(K+1)-1, \tag{3}$$

where $h(t)$ and $x_l(t)$ are the overall analytic passband impulse responses for the signal $\{s_n\}$ and the lth cyclostationary interferer $\{c_{n,l}\}$, $l = 1,\cdots,K$, respectively, and θ_l is a relative clock phase between the signal and the lth interferer, and T' is the sampling rate. The complex signal sequence $\{s_n\}$ and the lth complex interferer sequence $\{c_{n,l}\}$ are uncorrelated, and both sequences are white and have zero mean. It should be noted that the equalizer structure assumed for the analysis is the phase-splitting FSE (PS-FSE) [25], which combines the functions of a phase splitter and the equalizer. This PS-FSE has been used for implementing ATM-LAN, FTTC, and xDSL transmission systems [5], [9], [23]. With $K \times 100\%$ excess bandwidth to suppress all K interferers, the sampling rate for the real received signal should be greater than $2(K+1)/T$. Let $r(mT')$ be the value of $r(t)$ at the mth sampling instant, which is given by

$$r(mT') = \frac{1}{2}\sum_{n=-\infty}^{\infty}[s_n h(mT'-nT) + s_n^* h^*(mT'-nT)] + \frac{1}{2}\sum_{l=1}^{K}\sum_{n=-\infty}^{\infty}[c_{n,l}x_l(mT'-nT-\theta_l T') + c_{n,l}^* x_l^*(mT'-nT-\theta_l T')], \tag{4}$$

where the asterisk $(*)$ denotes the complex conjugate operation. Note from (4) that $r(mT')$ is determined by $h(mT')$, $h^*(mT')$, $x_l(mT')$, and $x_l^*(mT')$, whose spectra are $H(\omega)$, $H^*(-\omega)$, $X_l(\omega)$, and $X_l^*(-\omega)$, respectively. For a $2(K+1)/T$ equalizer that spans N symbols, and thus has $2N(K+1)$ taps, the input data vector at time nT is

$$\mathbf{r}(nT) = [r(nT+N(K+1)T'),\cdots,r(nT+T'), r(nT),\cdots,r(nT-N(K+1)T'+T')]^t, \tag{5}$$

where the superscript t denotes the transpose operation. The autocorrelation matrix $\mathbf{A}$ of $\mathbf{r}(nT)$ is given by

$$\mathbf{A} = E[\mathbf{r}(nT)\mathbf{r}^t(nT)]. \tag{6}$$

The characteristic equation of the autocorrelation matrix $\mathbf{A}$ is

$$\mathbf{A}\mathbf{v} = \lambda\mathbf{v}, \tag{7}$$

or, equivalently,

$$\sum_{i=-\infty}^{\infty} a(kT', iT')v_i = \lambda v_k, \quad k = -\infty,\cdots,\infty, \tag{8}$$

where $a(kT', iT')$ is the (k,i)th element of $\mathbf{A}$, λ is the eigenvalue associated with eigenvector $\mathbf{v}$ of $\mathbf{A}$, and v_i and v_k are the ith and kth elements of $\mathbf{v}$, respectively. Since the samples $r(mT')$ are cyclostationary with period of $2(K+1)$, the characteristic equation of (8) can be rewritten as

$$\begin{aligned}\sum_{i=-\infty}^{\infty} &[a_{r,0}((k-i)T)v_{2(K+1)i} \\ &+a_{r,1}((k-i)T)v_{2(K+1)i+1} \\ &+\cdots \\ &+a_{r,[2(K+1)-1]}((k-i)T)v_{2(K+1)i+[2(K+1)-1]}] \\ &= \lambda v_{2(K+1)k+r}, \\ &k = -\infty,\cdots,\infty;\ \ r = 0,1,\cdots,2(K+1)-1,\end{aligned} \tag{9}$$

where $a(kT+rT', iT+sT')$ depends only on the difference between k and i, thus being expressed as $a_{r,s}((k-i)T)$, $r,s = 0,1,\cdots,2(K+1)-1$. By taking the Fourier transform of (9), we have

$$\mathbf{A}(\omega)\mathbf{V}(\omega) = \lambda(\omega)\mathbf{V}(\omega), \tag{10}$$

where $\mathbf{V}(\omega) = [F(v_r)]^t$, $r = 0,1,\cdots,2(K+1)-1$, and $\mathbf{A}(\omega)$ is a $2(K+1)\times 2(K+1)$ matrix whose elements are $A_{r,s}(\omega) = F(a_{r,s}(nT))$, $r,s = 0,1,\cdots,2(K+1)-1$, and $F(\cdot)$ stands for the Fourier transform. From (4), (5), and (6), $\mathbf{A}(\omega)$ is computed as

$$\begin{aligned}\mathbf{A}(\omega) = &\mathbf{H}^{+*}(\omega)\mathbf{H}^{+t}(\omega) + \mathbf{H}^{-*}(\omega)\mathbf{H}^{-t}(\omega) \\ &+\mathbf{X}_1^{+*}(\omega)\mathbf{X}_1^{+t}(\omega) + \mathbf{X}_1^{-*}(\omega)\mathbf{X}_1^{-t}(\omega) \\ &+\mathbf{X}_2^{+*}(\omega)\mathbf{X}_2^{+t}(\omega) + \mathbf{X}_2^{-*}(\omega)\mathbf{X}_2^{-t}(\omega) \\ &+\cdots \\ &+\mathbf{X}_K^{+*}(\omega)\mathbf{X}_K^{+t}(\omega) + \mathbf{X}_K^{-*}(\omega)\mathbf{X}_K^{-t}(\omega),\end{aligned} \tag{11}$$

where $\mathbf{H}^+(\omega)$, $\mathbf{H}^-(\omega)$, $\mathbf{X}_l^+(\omega)$, and $\mathbf{X}_l^-(\omega)$, $l = 1,2,\cdots,K$, are $2(K+1)\times 1$ vectors whose elements are

$$H_r^+(\omega) = F(\frac{1}{2}h(nT-rT')),$$

$$X_{r+\theta_l}^+(\omega) = F(\frac{1}{2}x_l(nT-rT'-\theta_l T'))$$

$$H_r^-(\omega) = F(\frac{1}{2}h^*(nT-rT')),$$

$$X_{r+\theta_l}^-(\omega) = F(\frac{1}{2}x_l^*(nT-rT'-\theta_l T'))$$

$$r = 0, 1, \cdots, 2(K+1) - 1; \quad l = 1, 2, \cdots, K,$$

respectively. Note that there is no spectral overlap between $\mathbf{H}^+(\omega)$ (or $\mathbf{X}_l^+(\omega)$) and $\mathbf{H}^-(\omega)$ (or $\mathbf{X}_l^-(\omega)$). Thus, the vectors in (11) have the following orthogonal properties.

$$[\mathbf{H}^+(\omega), \mathbf{X}_l^+(\omega)] \perp [\mathbf{H}^-(\omega), \mathbf{X}_l^-(\omega)], \quad l = 1, 2, \cdots, K. \tag{12}$$

On the other hand, the vectors $\mathbf{H}^+(\omega)$ and $\mathbf{X}_l^+(\omega)$, $l = 1, 2, \cdots, K$, are correlated each other because they use the same frequency bands. Thus, the $K+1$ independent bases spanning the positive frequency component of $\mathbf{A}(\omega)$ can be represented by the linear combination of $\mathbf{H}^+(\omega)$ and $\mathbf{X}_l^+(\omega)$, $l = 1, 2, \cdots, K$. In a similar manner, the $K+1$ independent bases spanning the negative frequency component of $\mathbf{A}(\omega)$ can be obtained by the linear combination of $\mathbf{H}^-(\omega)$ and $\mathbf{X}_l^-(\omega)$, $l = 1, 2, \cdots, K$. Due to the orthogonal property between the positive and negative frequency components of $\mathbf{A}(\omega)$, the rank of $\mathbf{A}(\omega)$ is equal to $2(K+1)$. By using these $K+1$ positive and $K+1$ negative eigenvectors, we can obtain the $K+1$ positive and $K+1$ negative eigenvalues of $\mathbf{A}(\omega)$ as follows

$$\begin{aligned}&\mathbf{A}(\omega)[\alpha_{i,0}\mathbf{H}^{+*}(\omega) + \alpha_{i,1}\mathbf{X}_1^{+*}(\omega) + \cdots + \alpha_{i,K}\mathbf{X}_K^{+*}(\omega)] \\ &\quad = \lambda_i^+(\omega)[\alpha_{i,0}\mathbf{H}^{+*}(\omega) + \cdots + \alpha_{i,K}\mathbf{X}_K^{+*}(\omega)]\end{aligned} \tag{13}$$

$$\begin{aligned}&\mathbf{A}(\omega)[\beta_{i,0}\mathbf{H}^{-*}(\omega) + \beta_{i,1}\mathbf{X}_1^{-*}(\omega) + \cdots + \beta_{i,K}\mathbf{X}_K^{-*}(\omega)] \\ &\quad = \lambda_i^-(\omega)[\beta_{i,0}\mathbf{H}^{-*}(\omega) + \cdots + \beta_{i,K}\mathbf{X}_K^{-*}(\omega)] \\ &i = 0, 1, \cdots, K.\end{aligned} \tag{14}$$

From (11) and (13), we obtain (15), shown at the top of next page. Here, $\sum$ stands for $\sum_{r=0}^{2(K+1)-1}$. Similarly, from (11) and (14), we get (16), shown at the top of next page. With $K \times 100\%$ excess bandwidth, there exist the nontrivial solutions for $\{\alpha_0, \alpha_1, \cdots, \alpha_K\}$ and $\{\beta_0, \beta_1, \cdots, \beta_K\}$, i.e., the matrices $\mathbf{\Psi}^+(\omega)$ of (15) and $\mathbf{\Psi}^-(\omega)$ of (16) are singular. Note that the eigenvalue $\lambda^+(\omega)$ ($\lambda^-(\omega)$) in (15) ((16)) is equivalent to the eigenvalue of $\mathbf{\Phi}^+(\omega)$ ($\mathbf{\Phi}^-(\omega)$), defined as $\mathbf{\Phi}^+(\omega) \triangleq \mathbf{\Psi}^+(\omega) + \lambda^+(\omega)\mathbf{I}_{K+1}$ ($\mathbf{\Phi}^-(\omega) \triangleq \mathbf{\Psi}^-(\omega) + \lambda^-(\omega)\mathbf{I}_{K+1}$), where $\mathbf{I}_{K+1}$ denotes $(K+1) \times (K+1)$ identity matrix. By applying the Householder and Jacobi iteration methods [26], we can obtain the $K+1$ eigenvalues of $\lambda^+(\omega)$ for $\mathbf{\Phi}^+(\omega)$ and the $K+1$ eigenvalues of $\lambda^-(\omega)$ for $\mathbf{\Phi}^-(\omega)$, thus getting $2(K+1)$ eigenvalues of $\lambda(\omega)$ for $\mathbf{A}(\omega)$.

A.1 One Dominant Interferer

If there is one dominant interferer, the eigenvalues of $\mathbf{A}(\omega)$ are approximately obtained as

$$\mathbf{\Lambda}(\omega) = \begin{bmatrix} \lambda_1^-(\omega) & 0 & 0 & 0 \\ 0 & \lambda_0^-(\omega) & 0 & 0 \\ 0 & 0 & \lambda_0^+(\omega) & 0 \\ 0 & 0 & 0 & \lambda_1^+(\omega) \end{bmatrix}, \tag{17}$$

where

$$\lambda_0^+(\omega) = \sum_{r=0}^{3} |H_r^+(\omega)|^2 + CPS(H^+, X^+),$$

$$\lambda_1^+(\omega) = \sum_{r=0}^{3} |X_{r+\theta}^+(\omega)|^2 - CPS(H^+, X^+),$$

$$\lambda_0^-(\omega) = \sum_{r=0}^{3} |H_r^-(\omega)|^2 + CPS(H^-, X^-),$$

$$\lambda_1^-(\omega) = \sum_{r=0}^{3} |X_{r+\theta}^-(\omega)|^2 - CPS(H^-, X^-),$$

and $CPS(\cdot)$ denotes the cross power spectrum defined as

$$CPS(H^+, X^+) \triangleq \frac{|\sum_{r=0}^{3} H_r^+(\omega) X_{r+\theta}^{+*}(\omega)|^2}{\sum_{r=0}^{3} |H_r^+(\omega)|^2},$$

$$CPS(H^-, X^-) \triangleq \frac{|\sum_{r=0}^{3} H_r^-(\omega) X_{r+\theta}^{-*}(\omega)|^2}{\sum_{r=0}^{3} |H_r^-(\omega)|^2}.$$

In (17), we assumed that the signal-to-crosstalk power ratio (SNR) is high, i.e., $\sum_{r=0}^{3} |H_r^+(\omega)|^2 >> \sum_{r=0}^{3} |X_{r+\theta}^+(\omega)|^2$. Note from (17) that the four eigenvalues of $\mathbf{A}(\omega)$ are classified into $\lambda_0(\omega)$ and $\lambda_1(\omega)$. The eigenvalues $\lambda_0(\omega)$ ($\lambda_0^+(\omega)$ and $\lambda_0^-(\omega)$) are two large eigenvalues, which are computed by adding the folded signal power spectrum and the cross power spectrum between the signal and the interferer. The eigenvalues $\lambda_1(\omega)$ ($\lambda_1^+(\omega)$ and $\lambda_1^-(\omega)$) are two small eigenvalues, which are computed by subtracting the cross power spectrum from the folded interferer power spectrum. For a $4/T$ equalizer that spans N symbols, and thus has $4N$ taps, there exist $4N$ eigenvalues. Following from the argument given in [24], the $4N$ eigenvalues of $4N \times 4N$ autocorrelation matrix $\mathbf{A}$ are the uniformly spaced samples of $\lambda_0^+(\omega)$, $\lambda_1^+(\omega)$, $\lambda_1^-(\omega)$, and $\lambda_0^-(\omega)$, with N samples each.

A.2 Two Dominant Interferers

If there are two dominant interferers, the eigenvalues of $\mathbf{A}(\omega)$ are approximately computed as

$$\mathbf{\Lambda}(\omega) = \begin{bmatrix} \lambda_2^-(\omega) & 0 & 0 & 0 & 0 & 0 \\ 0 & \lambda_1^-(\omega) & 0 & 0 & 0 & 0 \\ 0 & 0 & \lambda_0^-(\omega) & 0 & 0 & 0 \\ 0 & 0 & 0 & \lambda_0^+(\omega) & 0 & 0 \\ 0 & 0 & 0 & 0 & \lambda_1^+(\omega) & 0 \\ 0 & 0 & 0 & 0 & 0 & \lambda_2^+(\omega) \end{bmatrix}, \tag{18}$$

where

$$\lambda_0^+(\omega) = \sum_{r=0}^{5} |H_r^+(\omega)|^2 + CPS(H^+, X_1^+) + CPS(H^+, X_2^+),$$

$$\begin{aligned}\lambda_1^+(\omega) = &\sum_{r=0}^{5} |X_{1,r+\theta_1}^+(\omega)|^2 \\ &- \frac{1}{2}[CPS(H^+, X_1^+) + CPS(H^+, X_2^+)] \\ &+ \frac{1}{2}[[CPS(H^+, X_1^+) + CPS(H^+, X_2^+)]^2\end{aligned}$$

$$\mathbf{\Psi}^{+}(\omega)\begin{bmatrix}\alpha_0\\ \alpha_1\\ \vdots\\ \alpha_K\end{bmatrix}=\begin{bmatrix}\sum|H_r^{+}(\omega)|^2-\lambda^{+}(\omega) & \sum H_r^{+}(\omega)X_{1,r+\theta_1}^{+*} & \cdots & \sum H_r^{+}(\omega)X_{K,r+\theta_K}^{+*}\\ \sum X_{1,r+\theta_1}^{+}H_r^{+*}(\omega) & \sum|X_{1,r+\theta_1}^{+}(\omega)|^2-\lambda^{+}(\omega) & \cdots & \sum X_{1,r+\theta_1}^{+}(\omega)X_{K,r+\theta_K}^{+*}\\ \vdots & \vdots & \ddots & \vdots\\ \sum X_{K,r+\theta_K}^{+}H_r^{+*}(\omega) & \sum X_{K,r+\theta_K}^{+}(\omega)X_{1,r+\theta_1}^{+*} & \cdots & \sum|X_{K,r+\theta_K}^{+}(\omega)|^2-\lambda^{+}(\omega)\end{bmatrix}\begin{bmatrix}\alpha_0\\ \alpha_1\\ \vdots\\ \alpha_K\end{bmatrix}=\mathbf{0} \tag{15}$$

$$\mathbf{\Psi}^{-}(\omega)\begin{bmatrix}\beta_0\\ \beta_1\\ \vdots\\ \beta_K\end{bmatrix}=\begin{bmatrix}\sum|H_r^{-}(\omega)|^2-\lambda^{-}(\omega) & \sum H_r^{-}(\omega)X_{1,r+\theta_1}^{-*} & \cdots & \sum H_r^{-}(\omega)X_{K,r+\theta_K}^{-*}\\ \sum X_{1,r+\theta_1}^{-}H_r^{-*}(\omega) & \sum|X_{1,r+\theta_1}^{-}(\omega)|^2-\lambda^{-}(\omega) & \cdots & \sum X_{1,r+\theta_1}^{-}(\omega)X_{K,r+\theta_K}^{-*}\\ \vdots & \vdots & \ddots & \vdots\\ \sum X_{K,r+\theta_K}^{-}H_r^{-*}(\omega) & \sum X_{K,r+\theta_K}^{-}(\omega)X_{1,r+\theta_1}^{-*} & \cdots & \sum|X_{K,r+\theta_K}^{-}(\omega)|^2-\lambda^{-}(\omega)\end{bmatrix}\begin{bmatrix}\beta_0\\ \beta_1\\ \vdots\\ \beta_K\end{bmatrix}=\mathbf{0} \tag{16}$$

$$+4CPS^2(X_1^{+},X_2^{+})-8CPS(H^{+},X_1^{+},X_2^{+})]^{1/2},$$

$$\lambda_2^{+}(\omega)=\sum_{r=0}^{5}|X_{2,r+\theta_2}^{+}(\omega)|^2-\frac{1}{2}[CPS(H^{+},X_1^{+})+CPS(H^{+},X_2^{+})]-\frac{1}{2}[[CPS(H^{+},X_1^{+})+CPS(H^{+},X_2^{+})]^2+4CPS^2(X_1^{+},X_2^{+})-8CPS(H^{+},X_1^{+},X_2^{+})]^{1/2},$$

$$\lambda_0^{-}(\omega)=\sum_{r=0}^{5}|H_r^{-}(\omega)|^2+CPS(H^{-},X_1^{-})+CPS(H^{-},X_2^{-}),$$

$$\lambda_1^{-}(\omega)=\sum_{r=0}^{5}|X_{1,r+\theta_1}^{-}(\omega)|^2-\frac{1}{2}[CPS(H^{-},X_1^{-})+CPS(H^{-},X_2^{-})]+\frac{1}{2}[[CPS(H^{-},X_1^{-})+CPS(H^{-},X_2^{-})]^2+4CPS^2(X_1^{-},X_2^{-})-8CPS(H^{-},X_1^{-},X_2^{-})]^{1/2},$$

$$\lambda_2^{-}(\omega)=\sum_{r=0}^{5}|X_{2,r+\theta_2}^{-}(\omega)|^2-\frac{1}{2}[CPS(H^{-},X_1^{-})+CPS(H^{-},X_2^{-})]-\frac{1}{2}[[CPS(H^{-},X_1^{-})+CPS(H^{-},X_2^{-})]^2+4CPS^2(X_1^{-},X_2^{-})-8CPS(H^{-},X_1^{-},X_2^{-})]^{1/2},$$

and $CPS(\cdot)$ denotes the cross power spectrum defined as

$$CPS(H^{+},X_1^{+})\triangleq\frac{|\sum_{r=0}^{5}H_r^{+}(\omega)X_{1,r+\theta_1}^{+*}(\omega)|^2}{\sum_{r=0}^{5}|H_r^{+}(\omega)|^2},$$

$$CPS(H^{+},X_2^{+})\triangleq\frac{|\sum_{r=0}^{5}H_r^{+}(\omega)X_{2,r+\theta_2}^{+*}(\omega)|^2}{\sum_{r=0}^{5}|H_r^{+}(\omega)|^2},$$

$$CPS(X_1^{+},X_2^{+})\triangleq\Big|\sum_{r=0}^{5}X_{1,r+\theta_1}^{+}(\omega)X_{2,r+\theta_2}^{+*}(\omega)\Big|,$$

$$CPS(H^{+},X_1^{+},X_2^{+})\triangleq\frac{1}{\sum_{r=0}^{5}|H_r^{+}(\omega)|^2}\times\mathrm{Re}\left[\sum_{r=0}^{5}\mathrm{H_r^{+}}(\omega)\mathrm{X_{1,r+\theta_1}^{+*}}(\omega)\sum_{r=0}^{5}\mathrm{X_{1,r+\theta_1}^{+}}(\omega)\mathrm{X_{2,r+\theta_2}^{+*}}(\omega)\times\sum_{r=0}^{5}X_{2,r+\theta_2}^{+}(\omega)H_r^{+*}(\omega)\right],$$

$$CPS(H^{-},X_1^{-})\triangleq\frac{|\sum_{r=0}^{5}H_r^{-}(\omega)X_{1,r+\theta_1}^{-*}(\omega)|^2}{\sum_{r=0}^{5}|H_r^{-}(\omega)|^2},$$

$$CPS(H^{-},X_2^{-})\triangleq\frac{|\sum_{r=0}^{5}H_r^{-}(\omega)X_{2,r+\theta_2}^{-*}(\omega)|^2}{\sum_{r=0}^{5}|H_r^{-}(\omega)|^2},$$

$$CPS(X_1^{-},X_2^{-})\triangleq\Big|\sum_{r=0}^{5}X_{1,r+\theta_1}^{-}(\omega)X_{2,r+\theta_2}^{-*}(\omega)\Big|,$$

$$CPS(H^{-},X_1^{-},X_2^{-})\triangleq\frac{1}{\sum_{r=0}^{5}|H_r^{-}(\omega)|^2}\times\mathrm{Re}\left[\sum_{r=0}^{5}\mathrm{H_r^{-}}(\omega)\mathrm{X_{1,r+\theta_1}^{-*}}(\omega)\sum_{r=0}^{5}\mathrm{X_{1,r+\theta_1}^{-}}(\omega)\mathrm{X_{2,r+\theta_2}^{-*}}(\omega)\times\sum_{r=0}^{5}X_{2,r+\theta_2}^{-}(\omega)H_r^{-*}(\omega)\right].$$

Note from (18) that the six eigenvalues $\lambda(\omega)$ of $\mathbf{A}(\omega)$ are classified into large ($\lambda_0^{-}(\omega)$ and $\lambda_0^{+}(\omega)$), middle ($\lambda_1^{-}(\omega)$ and $\lambda_1^{+}(\omega)$), and small ($\lambda_2^{-}(\omega)$ and $\lambda_2^{+}(\omega)$) eigenvalues. These eigenvalues depend on the folded signal power spectrum, the folded interferer power spectrum, the cross power spectrum between the signal and the interferer, and the cross power spectrum between the interferers. For a $6/T$ equalizer that spans N symbols, the $6N$ eigenvalues of autocorrelation matrix $\mathbf{A}$ are obtained by uniformly sampling $\lambda_0^{+}(\omega)$, $\lambda_1^{+}(\omega)$, $\lambda_2^{+}(\omega)$, $\lambda_2^{-}(\omega)$, $\lambda_1^{-}(\omega)$, and $\lambda_0^{-}(\omega)$, with N samples each. In Section III, these theoretical eigenvalues are compared with computer simulation results for multiuser application.

B. Iterative Equation of the Excess MSE

Using such an eigenstructure of the equalizer, we can now derive the iterative equation for the excess MSE in the presence of multiple cyclostationary interferers. It can be shown that the average MSE at nT is

$$\varepsilon(n) = E[e^2(n)] = \varepsilon_{min} + \varepsilon_{ex}(n), \tag{19}$$

where $e(n)$ is the complex error signal at the equalizer output, ε_{min} is the MMSE, and $\varepsilon_{ex}(n)$ is the excess MSE at nT. The MMSE is the average MSE obtained when the equalizer coefficient vector $\mathbf{C}(n)$ is the optimum, i.e., $\mathbf{C}(n) = \mathbf{C}_{opt}$ [15]. The excess MSE $\varepsilon_{ex}(n)$ is then equal to

$$\varepsilon_{ex}(n) = E[(\boldsymbol{\delta}\mathbf{C})^{*t}\mathbf{A}(\boldsymbol{\delta}\mathbf{C})], \tag{20}$$

where $\boldsymbol{\delta}\mathbf{C} = \mathbf{C}(n) - \mathbf{C}_{opt}$ is the coefficient-error vector at nT. The autocorrelation matrix $\mathbf{A}$ can be decomposed into the form

$$\begin{aligned}\mathbf{A} &= \mathbf{V}^{*t}\boldsymbol{\Lambda}\mathbf{V} \\ &= \mathbf{V}_0^{*t}\boldsymbol{\Lambda}_0\mathbf{V}_0 + \mathbf{V}_1^{*t}\boldsymbol{\Lambda}_1\mathbf{V}_1 + \cdots + \mathbf{V}_K^{*t}\boldsymbol{\Lambda}_K\mathbf{V}_K,\end{aligned} \tag{21}$$

where $\boldsymbol{\Lambda}$ is the $2N(K+1)\times 2N(K+1)$ diagonal matrix, which can be expressed as the sum of $K+1$ diagonal matrices $\boldsymbol{\Lambda}_i$,

$$\boldsymbol{\Lambda}_i = \begin{bmatrix} \mathbf{0} & & & & & & \\ & \ddots & & & & & \\ & & \mathbf{0} & & & & \\ & & & \mathbf{d}_i & & & \\ & & & & \mathbf{0} & & \\ & & & & & \ddots & \\ & & & & & & \mathbf{0} \end{bmatrix}.$$

and $\mathbf{d}_i$, $i = 0, 1, \cdots, K$, is the $2N \times 2N$ diagonal matrix whose elements are the uniformly spaced samples of $\lambda_i(\omega)$, and $\mathbf{V}_i$, $i = 0, 1, \cdots, K$, is the unitary matrix corresponding to $\boldsymbol{\Lambda}_i$. By defining the rotated coefficient-error vector $\mathbf{R}_i(n) = \mathbf{V}_i \cdot \boldsymbol{\delta}\mathbf{C}(n)$ and using (20) and (21), we can express the excess MSE $\varepsilon_{ex}(n)$ as

$$\begin{aligned}\varepsilon_{ex}(n) &= E[\mathbf{R}_0(n)^{*t}\boldsymbol{\Lambda}_0\mathbf{R}_0(n)] + E[\mathbf{R}_1(n)^{*t}\boldsymbol{\Lambda}_1\mathbf{R}_1(n)] \\ &\quad + \cdots + E[\mathbf{R}_K(n)^{*t}\boldsymbol{\Lambda}_K\mathbf{R}_K(n)] \\ &= \varepsilon_0(n) + \varepsilon_1(n) + \cdots + \varepsilon_K(n).\end{aligned} \tag{22}$$

From (22), we can now derive, with some approximations, the iterative equation for the excess MSE $\varepsilon_{ex}(n)$ in the presence of K interferers as follows:

$$\begin{aligned}\varepsilon_{ex}(n+1) &= \varepsilon_0(n+1) + \varepsilon_1(n+1) + \cdots + \varepsilon_K(n+1) \\ &\approx \varepsilon_0(n)[1 - 2\Delta\overline{\lambda}_0 + \Delta^2(2N)\lambda_{0,rms}^2] \\ &\quad + \varepsilon_{min}\Delta^2(2N)\lambda_{0,rms}^2 \\ &\quad + \varepsilon_1(n)[1 - 2\Delta\overline{\lambda}_1 + \Delta^2(2N)\lambda_{1,rms}^2] \\ &\quad + \varepsilon_{min}\Delta^2(2N)\lambda_{1,rms}^2 \\ &\quad + \cdots \\ &\quad + \varepsilon_K(n)[1 - 2\Delta\overline{\lambda}_K + \Delta^2(2N)\lambda_{K,rms}^2] \\ &\quad + \varepsilon_{min}\Delta^2(2N)\lambda_{K,rms}^2,\end{aligned} \tag{23}$$

where Δ is the step size of LMS algorithm, $\overline{\lambda}_i$ and $\lambda_{i,rms}$ are the mean and the root mean square (RMS) values of the eigenvalue set λ_i, $i = 0, 1, \cdots, K$, respectively. Note that λ_i represents $2N$ eigenvalues obtained by uniformly sampling $\lambda_i(\omega)$ ($\lambda_i^+(\omega)$ and $\lambda_i^-(\omega)$). Note also from (23) that the total excess MSE $\varepsilon_{ex}(n)$ of the equalizer can be expressed by the sum of the $K+1$ excess MSEs, $\varepsilon_j(n)$, $j = 0, 1, \cdots, K$, which are determined by $K+1$ different eigenvalue sets. In order for the excess MSE to decay, the step size Δ must satisfy the inequalities

$$0 \le \Delta \le \frac{2\overline{\lambda}_j}{(2N)\lambda_{j,rms}^2} \quad \text{for} \quad \varepsilon_j(n), \quad j = 0, 1, \cdots, K. \tag{24}$$

Since $\lambda_0 > \lambda_1 > \cdots > \lambda_K$, the convergence bound of the total excess MSE becomes

$$0 \le \Delta \le \frac{2\overline{\lambda}_0}{(2N)\lambda_{0,rms}^2} = \Delta_{max}. \tag{25}$$

It can be shown from [24] that the optimum step size for the fastest initial convergence is $\Delta_{opt} = \Delta_{max}/2$. In the transient region, $\varepsilon_K(n)$ is the largest among $\varepsilon_j(n)$, $j = 0, 1, \cdots, K$, and thus $\varepsilon_{ex}(n) \approx \varepsilon_K(n)$, i.e.,

$$\begin{aligned}\varepsilon_{ex}(n+1) &\approx \varepsilon_K(n+1) \\ &= \varepsilon_K(n)[1 - 2\Delta_{opt}\overline{\lambda}_K + \Delta_{opt}^2(2N)\lambda_{K,rms}^2] \\ &\quad + \varepsilon_{min}\Delta_{opt}^2(2N)\lambda_{K,rms}^2 \\ &\approx \varepsilon_K(n)\left[1 - \frac{2\overline{\lambda}_0\overline{\lambda}_K}{(2N)\lambda_{0,rms}^2}\right] \\ &\quad + \varepsilon_{min}\frac{(\overline{\lambda}_0)^2\lambda_{K,rms}^2}{(2N)(\lambda_{0,rms}^2)^2}.\end{aligned} \tag{26}$$

From (26), we see that if $\Delta = \Delta_{opt}$, the equalizer converges according to $[1 - \frac{2\overline{\lambda}_0\overline{\lambda}_K}{(2N)\lambda_{0,rms}^2}]^n$ approximately. In the steady-state region, $\varepsilon_0(n)$ is the largest among $\varepsilon_j(n)$, $j = 0, 1, \cdots, K$, and thus $\varepsilon_{ex}(\infty) \approx \varepsilon_0(\infty)$. That is,

$$\begin{aligned}\varepsilon_{ex}(\infty) &\approx \varepsilon_0(\infty) \\ &= \varepsilon_0(\infty)[1 - 2\Delta\overline{\lambda}_0 + \Delta^2(2N)\lambda_{0,rms}^2] \\ &\quad + \varepsilon_{min}\Delta^2(2N)\lambda_{0,rms}^2.\end{aligned} \tag{27}$$

Hence, with the optimum step size, the steady-state excess MSE $\varepsilon_{ex}(\infty)$ is computed as

$$\varepsilon_{ex}(\infty) \approx \varepsilon_0(\infty) = \varepsilon_{min}\frac{\Delta_{opt}(2N)\lambda_{0,rms}^2}{2\overline{\lambda}_0 - \Delta_{opt}(2N)\lambda_{0,rms}^2} = \varepsilon_{min}. \tag{28}$$

In other words, when the step size is equal to Δ_{opt}, the steady-state MSE is 3 dB higher than the MMSE. In Section III, this peculiar convergence characteristic in the presence of cyclostationary interference is investigated for high-speed LAN and xDSL applications.

C. MMSE Expression Using the Equalizer's Eigenstructure

In this subsection, we formulate the MMSE in the presence of multiple cyclostationary interference, by using the equalizer's

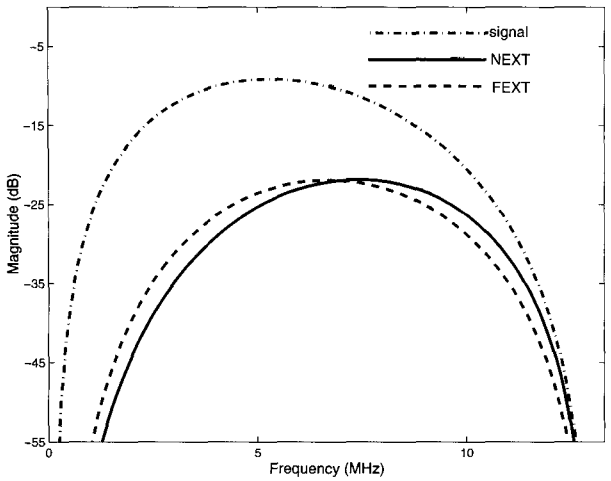

Fig. 3. Spectra of the 16-CAP/QAM signal, NEXT, and FEXT at the output of a 1kft 24 gauge loop (the power level of FEXT is boosted so that the signal-to-FEXT power ratio is the same as the signal-to-NEXT power ratio at the input of the receiver).

eigenstructure, i.e., the folded signal, interferer power spectra, and their cross power spectra. As will be shown in Section III, this MMSE expression is useful to investigate the performance in the presence of cyclostationary interference having different power spectra, as is the case for high-speed LAN and xDSL systems in the presence of NEXT and FEXT. From [1], the MMSE of $K+1$ input, $K+1$ output, multiuser communication system can be expressed as

$$\varepsilon_{min} = \frac{N_0}{\sigma_d^2} \cdot \frac{1}{2\pi} \int_{-\pi}^{\pi} \mathrm{tr}\left([\frac{N_0}{\sigma_d^2}\mathbf{I}_{K+1} + \mathbf{\Phi}(\omega)]^{-1} \right) d\omega, \quad (29)$$

where tr(·) stands for the trace of a matrix and σ_d^2 and N_0 are variances of the signal and background noise, respectively. By defining

$$\mathbf{Q}(\omega) \triangleq \frac{N_0}{\sigma_d^2}\mathbf{I}_{K+1} + \mathbf{\Phi}(\omega), \quad (30)$$

the MMSE expression of (29) can be rewritten as

$$\begin{aligned} \varepsilon_{min} &= \frac{N_0}{\sigma_d^2} \cdot \frac{1}{2\pi} \int_{-\pi}^{\pi} \mathrm{tr}(\mathbf{Q}^{-1}(\omega)) d\omega \quad (31) \\ &= \frac{N_0}{\sigma_d^2} \cdot \frac{1}{2\pi} \int_{-\pi}^{\pi} \frac{\mathbf{Q}_{1,1}(\omega)}{\mathrm{det}\mathbf{Q}(\omega)} d\omega + \cdots \\ &+ \frac{N_0}{\sigma_d^2} \cdot \frac{1}{2\pi} \int_{-\pi}^{\pi} \frac{\mathbf{Q}_{K+1,K+1}(\omega)}{\mathrm{det}\mathbf{Q}(\omega)} d\omega \\ &= MMSE(\text{user 0}) + \cdots + \text{MMSE(user K)}, \end{aligned}$$

where $\mathrm{det}\mathbf{Q}(\omega)$ stands for the determinant of $\mathbf{Q}(\omega)$ and the cofactor $\mathbf{Q}_{i,j}(\omega)$ is defined as $\mathbf{Q}_{i,j}(\omega) \triangleq (-1)^{i+j}\mathrm{det}\mathbf{M}_{i,j}(\omega)$ with $\mathbf{M}_{i,j}(\omega)$ being formed by deleting row i and column j of $\mathbf{Q}(\omega)$. For instance, the MMSE at the 'user 0' receiver with one cyclostationary interferer is expressed as

$$\varepsilon_{min}(\text{user 0}) = \frac{\mathrm{N_0}}{\sigma_\mathrm{d}^2} \cdot \frac{1}{2\pi} \int_{-\pi}^{\pi} \frac{\mathbf{Q}_{1,1}(\omega)}{\mathrm{det}\mathbf{Q}(\omega)} \mathrm{d}\omega, \quad (32)$$

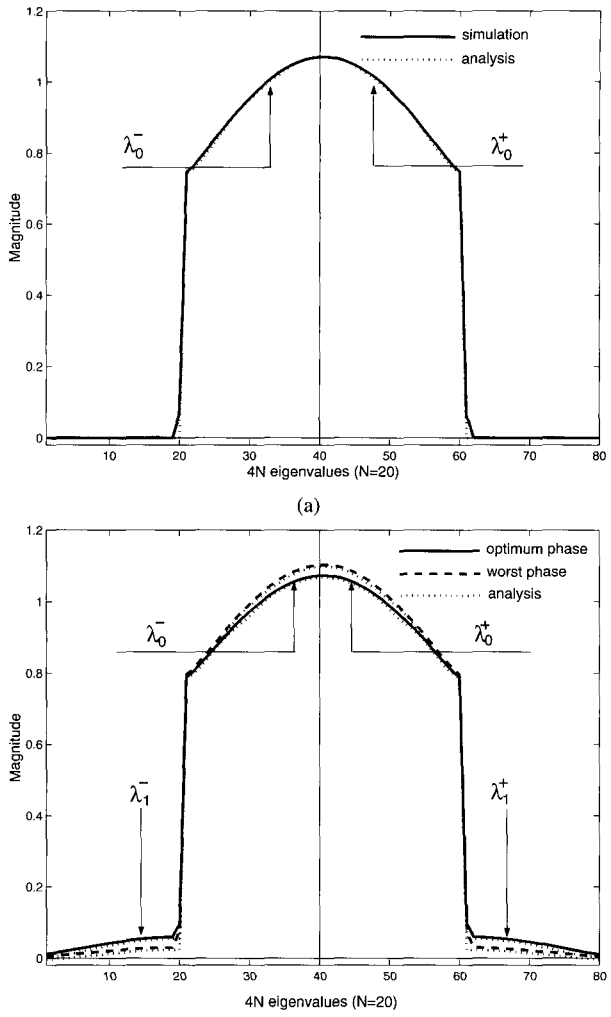

Fig. 4. Eigenvalues in the presence of stationary noise or a cyclostationary NEXT for the same SNR at the input of the receiver: (a) Stationary noise. (b) cyclostationary NEXT (optimum and worst relative phases).

where

$$\begin{aligned} \frac{\mathbf{Q}_{1,1}(\omega)}{\mathrm{det}\mathbf{Q}(\omega)} &= \left[\left(\frac{N_0}{\sigma_d^2} + \sum_{r=0}^{3} |H_r(\omega)|^2 \right) \right. \\ &\left. - \left(\sum_{r=0}^{3} |H_r(\omega)|^2 \right) \frac{CPS(H,X)}{(\frac{N_0}{\sigma_d^2} + \sum_{r=0}^{3} |X_{r+\theta}(\omega)|^2)} \right]^{-1} \\ &\approx \frac{1}{\mathrm{SNR_i}(\omega)\lambda_1(\omega)}, \end{aligned}$$

where $\mathrm{SNR}_i(\omega) \triangleq \sum_{r=0}^{3} |H_r(\omega)|^2 / \sum_{r=0}^{3} |X_{r+\theta}(\omega)|^2$. Note from (32) that the MMSE is determined by the small eigenvalue $\lambda_1(\omega)$. Note also from the denominator in (32) that the cross power spectrum $CPS(H,X)$ is amplified by the SNR ratio, i.e., $\mathrm{SNR}_i(\omega)$, thus making the MMSE very sensitive to the correlation between the signal and the interference. Specifically, the MMSE increases as the interference spectrum becomes similar to the signal spectrum. If there are two interferers, the integrand in (32) can be rewritten as (33), shown at the top of this

$$\frac{\mathbf{Q}_{1,1}(\omega)}{\det\mathbf{Q}(\omega)} = \frac{1}{(\frac{N_0}{\sigma_d^2}+\sum_{r=0}^{5}|H_r(\omega)|^2)-(\sum_{r=0}^{5}|H_r(\omega)|^2)\frac{(\frac{N_0}{\sigma_d^2}+\sum_{r=0}^{5}|X_{1,r+\theta_1}(\omega)|^2)CPS(H,X_2)+(\frac{N_0}{\sigma_d^2}+\sum_{r=0}^{5}|X_{2,r+\theta_2}(\omega)|^2)CPS(H,X_1)-2CPS(H,X_1,X_2)}{(\frac{N_0}{\sigma_d^2}+\sum_{r=0}^{5}|X_{1,r+\theta_1}(\omega)|^2)(\frac{N_0}{\sigma_d^2}+\sum_{r=0}^{5}|X_{2,r+\theta_2}(\omega)|^2)-CPS^2(X_1,X_2)}}. \quad (33)$$

Table 1. Average and root mean square values of the eigenvalues in the presence of NEXT or FEXT (optimum and worst relative phases).

	relative phase	$\overline{\lambda_0}$	$\lambda_{0,rms}$	$\overline{\lambda_1}$	$\lambda_{1,rms}$
NEXT	optimum phase (ϕ_2)	0.9571	0.9768	0.0257	0.0330
NEXT	worst phase (ϕ_0)	0.9697	0.9881	0.0117	0.0151
FEXT	optimum phase (φ_2)	0.9610	0.9828	0.0214	0.0279
FEXT	worst phase (φ_0)	0.9756	0.9954	0.0053	0.0070

Table 2. Steady-state performance of the equalizer in the presence of NEXT or FEXT ($\varepsilon(\infty) = \varepsilon_{ex}(\infty) + \varepsilon_{min} = \varepsilon_0(\infty) + \varepsilon_1(\infty) + \varepsilon_{min}$).

	relative phase	$\overline{CPS(H,X)}$	$\varepsilon_0(\infty)$(dB)	$\varepsilon_1(\infty)$(dB)	$\varepsilon_{ex}(\infty)$(dB)	ε_{min}(dB)	$\varepsilon(\infty)$(dB)
NEXT	optimum phase (ϕ_2)	0.0492	−50.42	−67.05	−50.33	−50.42	−47.36
NEXT	worst phase (ϕ_0)	0.0634	−47.17	−67.27	−47.13	−47.17	−44.14
FEXT	optimum phase (φ_2)	0.0535	−48.69	−66.04	−48.61	−48.69	−45.64
FEXT	worst phase (φ_0)	0.0698	−42.06	−65.46	−42.04	−42.06	−39.04

page. In the next section, the steady-state performance for multiuser communication system is discussed by using this MMSE expression.

III. PERFORMANCE OF MULTIUSER WIRED COMMUNICATION SYSTEM

In this section, we evaluate the performance of cyclostationary interference suppression for multi-user wired communication systems and verify the theoretical receiver behaviors in the following three different scenarios.

A. NEXT/FEXT Suppression

In this subsection, we investigate the convergence and steady-state behaviors of the equalizer in the presence of a cyclostationary crosstalk interference. We also compare the cyclostationary crosstalk suppression for NEXT and FEXT, and show that FEXT is more difficult to suppress than NEXT for the same SNR at the input of the receiver. In ATM-LAN environment, NEXT is usually much more severe than FEXT [5] whereas, for VDSL environment, FEXT is a major impairment because of the nonoverlapping frequency bands for the downstream and upstream channels [3], [9]–[12]. VDSL is considered as the next generation ADSL technology, delivering multimegabit data rates (up to 51.84 Mb/s) over ordinary phone lines to customers [10], [11]. Refer to [5] and [9] for details on the propagation loss and NEXT/FEXT characteristics in ATM-LAN and broadband access environments.

Fig. 3 shows the spectra of 25.92 Mb/s 16-CAP/QAM signal, NEXT and FEXT, which have propagated through 1kft 24 gauge loop. In Fig. 3, the power level of FEXT is boosted so that the signal-to-FEXT power ratio is the same as the signal-to-NEXT power ratio at the input of the receiver, which is 12.17 dB. Fig. 4 gives the eigenvalues of the equalizer in the presence of stationary noise or a cyclostationary NEXT, where the equalizer used a memory span of $N = 20$ symbols, and thus had 80 taps. Note from Fig. 4 that, unlike the equalizer in a stationary noise environment, where there are $2N$ nonzero eigenvalues [25], there are $4N$ nonzero eigenvalues in the presence of a cyclostationary interferer. This is due to the fact that the rank of $\mathbf{A}(\omega)$ in (11) is equal to four, whereas the rank of $\mathbf{A}(\omega)$ is two in the presence of stationary noise. Notice also from Fig. 4 that theoretical eigenvalues obtained by computing (17) are consistent with computer simulation results. Fig. 5(a) shows the convergence characteristics of the equalizer in the presence of stationary noise or a cyclostationary interference, which are obtained through computer simulation and analysis. It should be noted from Figs. 4 and 5(a) that the equalizer's eigenvalues in the presence of cyclostationary interference are comprised of two different eigenvalues, i.e., large (λ_0) and small (λ_1) eigenvalues, thus exhibiting significantly different initial convergence and steady-state behaviors as compared to the one in the presence of stationary noise. The solid lines in Fig. 5(a) represent the convergence behavior with the optimum and worst relative clock phases between the signal and the cyclostationary crosstalk. The optimum and worst phases represent the relative phase of the symbol clocks used by the signal and the interferers, which yield the optimum and worst steady-state performances, respectively. The different phases ϕ_i ($i = 0, 1, 2, 3$) are obtained by shifting the relative phase of the clocks of the disturbed and disturbing signals by multiples of the sampling period T'. This relative phase influences the performance because of the cyclostationarity nature of the two signals. Fig. 5(b) shows the excess MSE of (23) and the MMSE of (32), which explains the convergence behavior shown in Fig. 5(a). Table 1 summarizes the average and RMS eigenvalues in the presence of a cyclostationary NEXT or FEXT (optimum and worst relative phases). As seen in Table 1, for the NEXT case, the average of the large

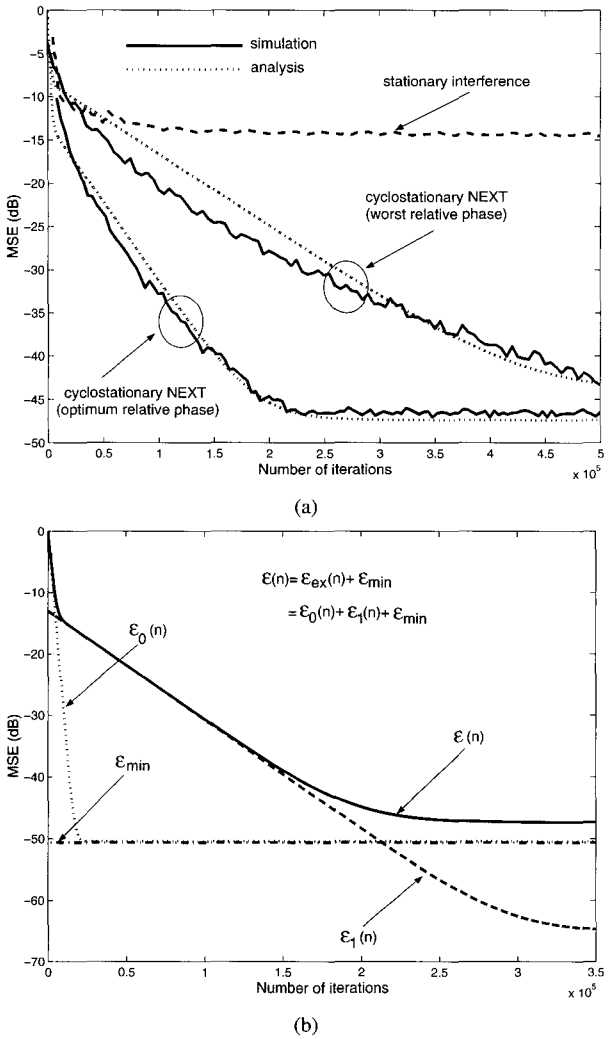

Fig. 5. (a) Convergence behavior of the equalizer in the presence of stationary noise or a cyclostationary NEXT for the same SNR at the input of the receiver. (b) Analysis of the MSE for a cyclostationary NEXT (optimum relative phase).

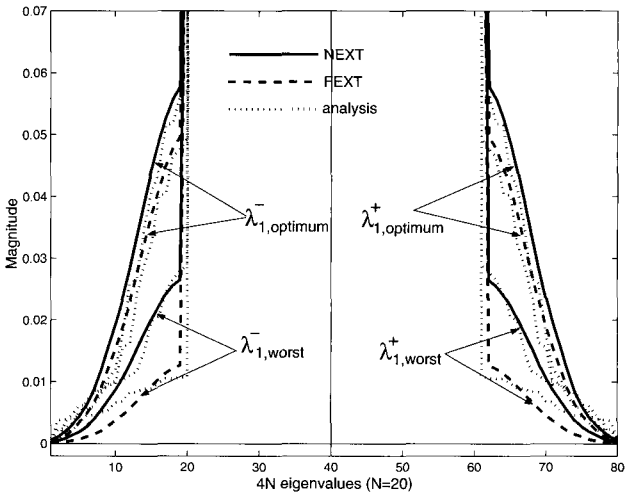

Fig. 6. Comparison of the small eigenvalue (λ_1) for cyclostationary NEXT and FEXT.

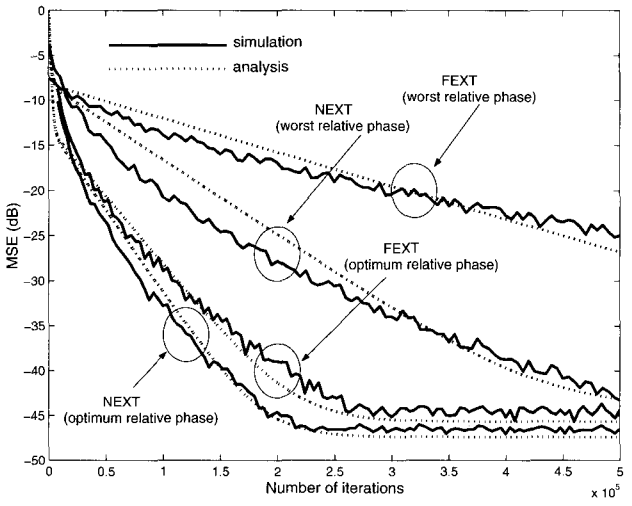

Fig. 7. Convergence behavior of the equalizer in the presence of a cyclostationary NEXT or FEXT (computer simulation and theoretical analysis).

eigenvalues, $\overline{\lambda}_0$, is almost the same for both the optimum and worst phases ($\overline{\lambda}_{0,optimum} = 0.9571$, $\overline{\lambda}_{0,worst} = 0.9697$), but the average of the small eigenvalues, $\overline{\lambda}_1$, of the worst phase is about half that of the optimum phase ($\overline{\lambda}_{1,optimum} = 0.0257$, $\overline{\lambda}_{1\ worst} = 0.0117$). Note from (26) that the equalizer converges according to $[1 - \frac{2\overline{\lambda}_0\overline{\lambda}_1}{(2N)\lambda^2_{0,rms}}]^n$. Therefore, the convergence time with the worst phase is about twice as long as the one with the optimum phase, as shown in Fig. 5(a). Table 2 gives the steady-state performance of the equalizer, which is obtained by adding the excess MSE $\varepsilon_{ex}(\infty)$ of (28) and the MMSE of (32), i.e., $\varepsilon(\infty) = \varepsilon_{ex}(\infty) + \varepsilon_{min} = \varepsilon_0(\infty) + \varepsilon_1(\infty) + \varepsilon_{min} \approx \varepsilon_0(\infty) + \varepsilon_{min}$. With the step size $\Delta_{opt} = \Delta_{max}/2$, we have the steady-state performance $\varepsilon(\infty) \approx 2 \times \varepsilon_{min}$. Note from (32) that the MMSE degrades as the small eigenvalue λ_1 decreases. Hence, the steady-state performance with the worst phase is about 3 dB worse than that with the optimum phase because the average of the small eigenvalues, $\overline{\lambda}_1$, of the worst phase is about half that of the optimum phase. Table 2 also compares the steady-state performance for the NEXT and FEXT cases. Note from (32) that the MMSE ε_{min} is strongly dependent upon the cross power spectrum $CPS(H, X)$ between the signal and the interferer. In other words, the MMSE degrades as the cross power spectrum increases. The first column in the table gives the average cross power spectrum of NEXT/FEXT. Notice from Fig. 3 that the FEXT spectrum is more similar to the signal spectrum than the NEXT spectrum is, which results in an increase in the cross power spectrum between the signal and the interferer for the FEXT case. Therefore, the steady-state performance in the presence of FEXT (VDSL environment) is worse than that in the presence of NEXT (ATM-LAN environment) for the same SNR at the input of the receiver. Figs. 6 and 7 compare the small eigenvalue λ_1 of cyclostationary NEXT and FEXT, and their convergence behaviors, respectively. Computer simulation result indicates that the performance in the presence of FEXT degrades by 4.1 dB as compared to the NEXT case, which is consistent with the analytical result of 5.1 dB, obtained from the worst phase in Table 2.

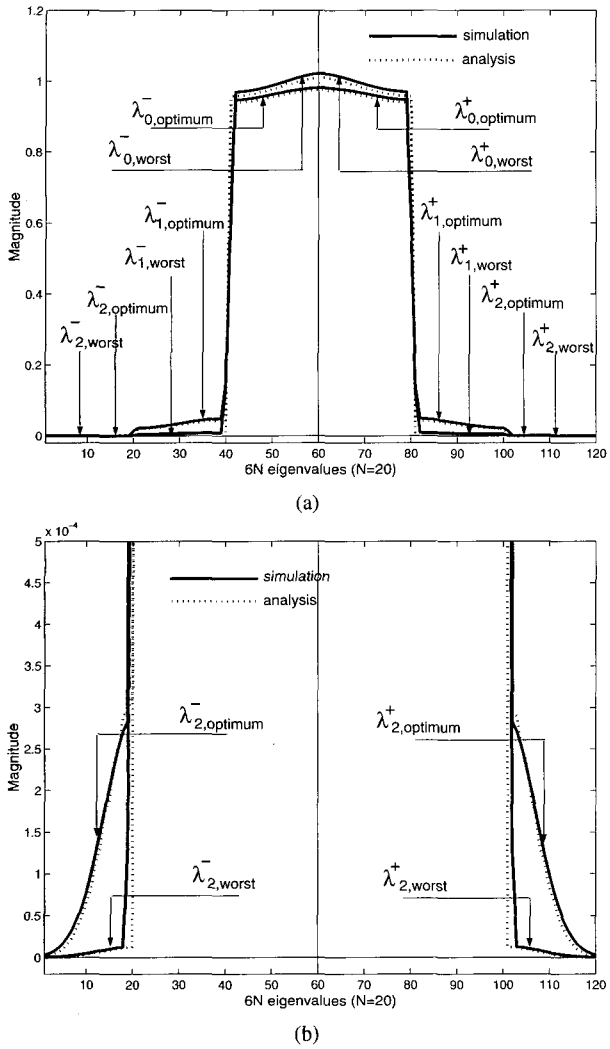

Fig. 8. (a) Eigenvalues in the presence of two cyclostationary interferers (NEXT and FEXT) for the optimum (ϕ_4, φ_3) and worst (ϕ_0, φ_0) relative phases. (b) Small eigenvalue (λ_2) in Fig. 8(a).

B. *Suppression of Two Different Cyclostationary Interferers: NEXT and FEXT*

In this subsection, we investigate the performance of the equalizer in the presence of two different cyclostationary interferers. In this case, we use an idealized model for NEXT and FEXT characteristics. Fig. 8(a) gives the eigenvalues of $6/T$ equalizer when the 16-CAP/QAM signal with 200% excess bandwidth has propagated through 600 ft 24 gauge cable in the presence of NEXT and FEXT. The signal-to-NEXT plus FEXT power ratio was 10.28 dB. Notice from Fig. 8(a) that the $6N$ eigenvalues are classified into large (λ_0), middle (λ_1), and small (λ_2) eigenvalues. Fig. 8(b) shows a detailed figure for the eigenvalue λ_2 in Fig. 8(a). Table 3 summarizes the average eigenvalues and the average cross power spectra in the presence of NEXT and FEXT. Since $CPS(H, X_i) >> CPS^2(X_1, X_2)$ and $CPS(H, X_i) >> CPS(H, X_1, X_2)$, $i = 1, 2$, the MMSE in the presence of two interferers (see (33)) is approximately

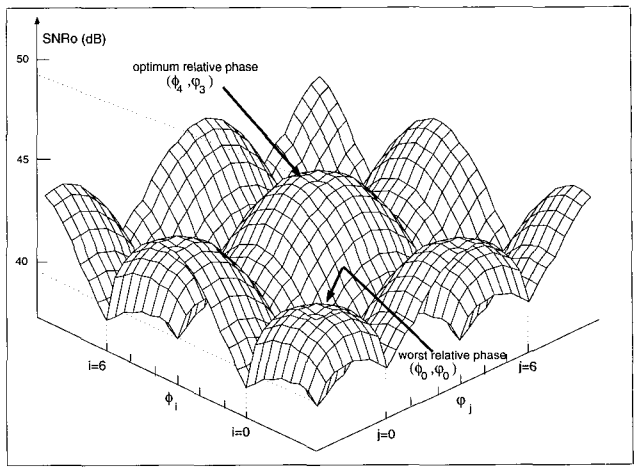

Fig. 9. Steady-state MSE in the presence of cyclostationary NEXT and FEXT interferers for all relative phases.

computed as

$$\varepsilon_{min} \approx \frac{N_0}{\sigma_d^2} \cdot \frac{1}{2\pi} \int_{-\pi}^{\pi} \frac{1}{2\mathrm{SNR}_i(\omega)\lambda_2(\omega)} d\omega \tag{34}$$

where $\mathrm{SNR}_i(\omega) \triangleq (\sum_{r=0}^{5} |H_r(\omega)|^2)/(\sum_{r=0}^{5} |X_{1,r+\theta_1}(\omega)|^2 + \sum_{r=0}^{5} |X_{2,r+\theta_2}(\omega)|^2)$. Note from (34) that among all relative phases, the relative phases having the largest and smallest values of λ_2 yield the optimum and worst steady-state performances, respectively. Fig. 9 shows computer simulation result for the steady-state performance in the presence of NEXT and FEXT for all relative phases. The optimum and worst relative phases in Fig. 9 are (ϕ_4, φ_3) and (ϕ_0, φ_0), respectively, where $\phi_i = i \times \frac{T}{6}$ ($i = 0, 1, \cdots, 5$), and $\varphi_j = j \times \frac{T}{6}$ ($j = 0, 1, \cdots, 5$) stand for the relative phase of the symbol clocks used by the signal and NEXT, and by the signal and FEXT, respectively. Note from Table 3 that the eigenvalue λ_2 with the optimum phase is 9.56 times larger than that with the worst phase ($\bar{\lambda}_{2,optimum} = 1.5298 \times 10^{-4}$, $\bar{\lambda}_{2,worst} = 1.6010 \times 10^{-5}$), which results in about 10 dB performance difference between the optimum and worst relative phases, as shown in Fig. 9 and Table 4. Fig. 10(a) shows the convergence characteristics of the equalizer in the presence of NEXT and FEXT, which are obtained through computer simulation and analysis. The convergence speed with the optimum phase is about 10 times faster than that with the worst phase, which can be predicted from the analysis in (26). Notice from Fig. 10(a) that there is a discrepancy between the analysis and the simulation result for the optimum relative phase. This occurs because the small (λ_2) eigenvalues have somewhat large variation around the average value of $\bar{\lambda}_2$ for the optimum relative phase case. Fig. 10(b) gives the excess MSE, $\varepsilon_0(n)$, $\varepsilon_1(n)$, and $\varepsilon_2(n)$, and the MMSE of (33), explaining the analytical convergence behavior shown in Fig. 10(a). Notice from [5] that the transceiver equalizes both the signal and the interferers, but in a different fashion. The sampled values of the overall impulse response for the signal, which includes the transmitter, the channel, and the equalizer, are zero at all the multiples of the symbol period, except the origin, whereas the sampled values of the overall impulse responses for NEXT and FEXT are zero

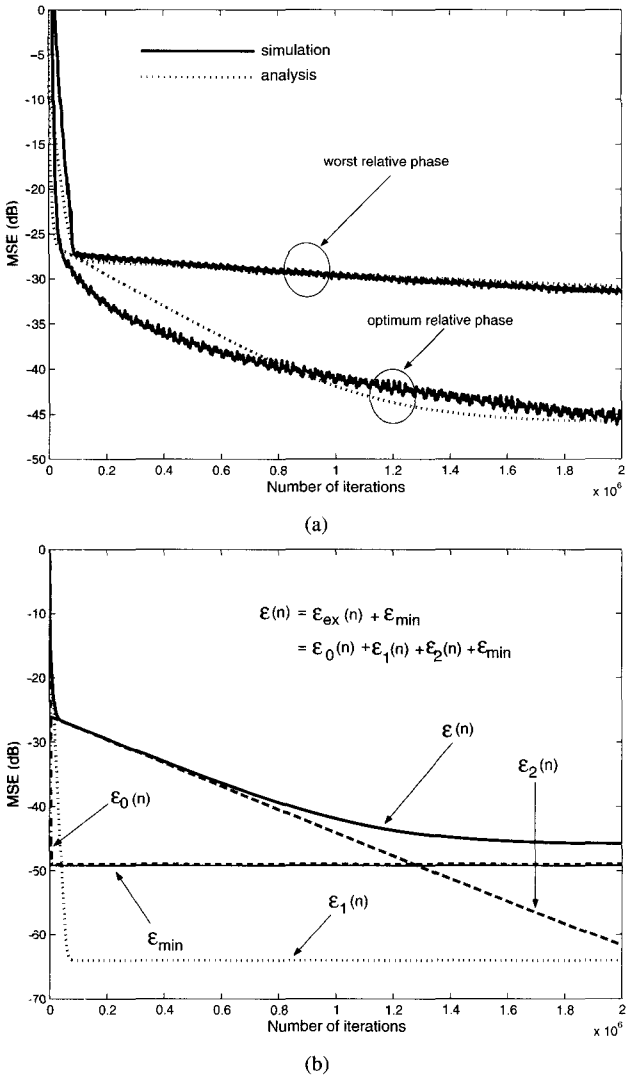

Fig. 10. (a) Convergence behavior of the equalizer in the presence of two cyclostationary interferers (NEXT and FEXT). (b) Analysis of the MSE (optimum relative phase).

at all the multiples of the symbol period, including the origin. As such, with 200% excess bandwidth, the equalizer eliminates the intersymbol interference of the signal and at the same time suppresses both NEXT and FEXT.

C. Suppression of Two NEXTs with Measured Characteristics

In this subsection, we investigate the performance of the equalizer in the presence of two NEXTs. In this case, measured NEXT characteristics are used instead of an idealized NEXT model. When the relative phases of the symbol clocks used by the signal and the interferers are the same, i.e., $\phi_i = \varphi_i$, $i = 0, 1, \cdots, 5$, the system arrangement with two model NEXTs is converged into the one NEXT interferer case because two interferers go through an identical NEXT transfer function. Thus, the analysis with an idealized model could not be used to predict the system performance in realistic environment. Fig. 11 shows the spectra of 25.92 Mb/s 16-CAP/QAM signal and two NEXTs, obtained by using the measured 25-pair BKMA 600 ft cable

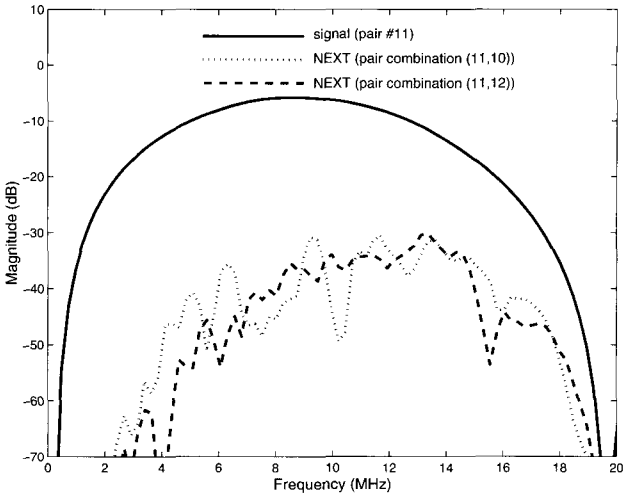

Fig. 11. Spectra of the 16-CAP/QAM signal, and two worst case pair-to-pair measured NEXTs at the output of a 600ft BKMA cable.

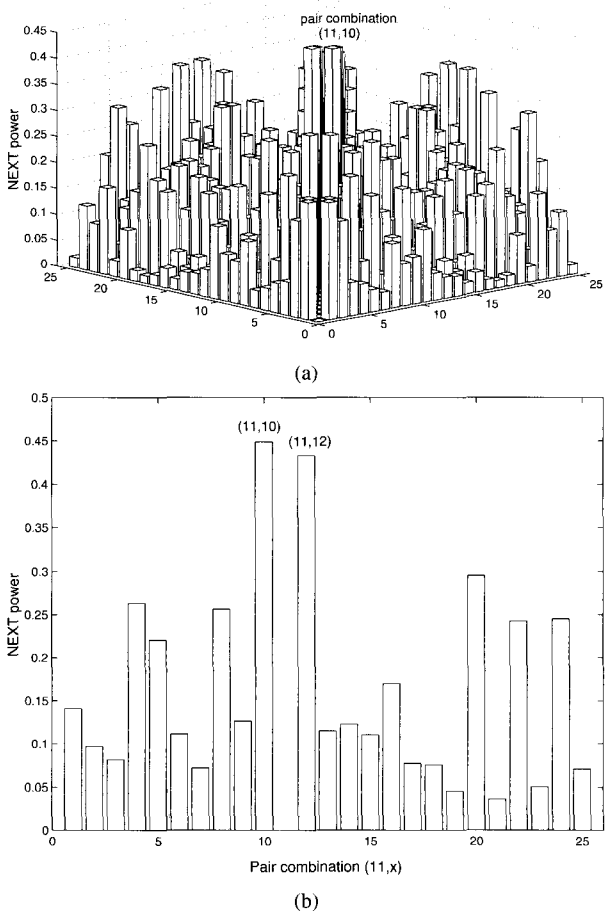

Fig. 12. (a) Measured pair-to-pair NEXT power of 25-pair BKMA cable. (b) Measured pair-to-pair NEXT power for the pair #11.

characteristics, which is a typical 24 gauge distribution loop for broadband access. The signal-to-two measured NEXTs power ratio was 23.53 dB. Fig. 12(a) shows the measured pair-to-pair NEXT power, which is obtained by integrating the NEXT loss over the frequencies used for the signal. Fig. 12(b) shows the

Table 3. Average eigenvalues and cross power spectra in the presence of NEXT and FEXT.

relative phase	$\overline{\lambda_0}$	$\overline{\lambda_1}$	$\overline{\lambda_2}$	$\overline{CPS(H,X_1)}$	$\overline{CPS(H,X_2)}$	$\overline{CPS(X_1,X_2)}$	$\overline{CPS(H,X_1,X_2)}$
optimum phase (ϕ_4,φ_3)	0.9467	0.0405	1.5298×10^{-4}	0.0153	0.0015	0.0143	6.2408×10^{-5}
worst phase (ϕ_0,φ_0)	0.9747	0.0129	1.6010×10^{-5}	0.0371	0.0048	0.0150	2.0125×10^{-4}

Table 4. Steady-state performance of the equalizer in the presence of NEXT and FEXT.
($\varepsilon(\infty) = \varepsilon_{ex}(\infty) + \varepsilon_{min} = \varepsilon_0(\infty) + \varepsilon_1(\infty) + \varepsilon_2(\infty) + \varepsilon_{min}$).

relative phase	$\varepsilon_0(\infty)$(dB)	$\varepsilon_1(\infty)$(dB)	$\varepsilon_2(\infty)$(dB)	$\varepsilon_{ex}(\infty)$(dB)	ε_{min}(dB)	$\varepsilon(\infty)$(dB)
optimum phase (ϕ_4, φ_3)	−48.98	−64.06	−89.76	−48.82	−48.98	−45.89
worst phase (ϕ_0, φ_0)	−39.51	−53.84	−82.27	−39.35	−39.51	−36.42

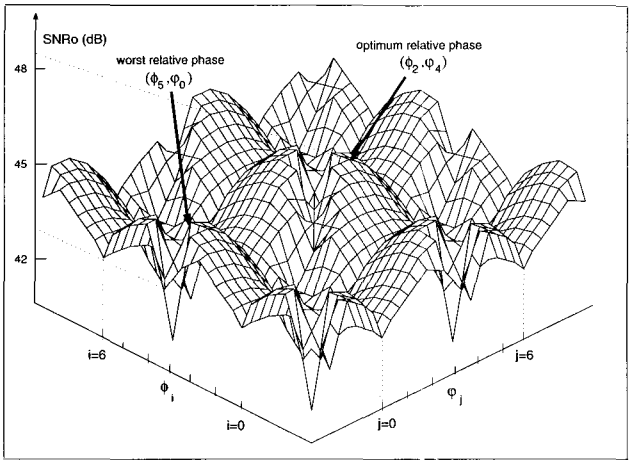

Fig. 13. Steady-state performance in the presence of two worst-case measured NEXTs for all relative phases.

NEXT power when the NEXT is measured at a receiver located at the end of pair #11. Note that, when multiple NEXT interferers are present, there are always dominant interferers, which are pair combinations (11, 10) and (11, 12) for the pair #11. The wavy NEXT curves in Fig. 11 were generated by using these two worst-case pair-to-pair measured NEXT characteristics. Analysis and computer simulation results indicate that, among all the relative phases, the eigenvalues λ_2 with the relative phases (ϕ_2, φ_4) and (ϕ_5, φ_0) are the largest and smallest values, which yield the optimum and worst steady-state performances, respectively. Fig. 13 gives steady-state performance in the presence of two worst-case measured NEXTs for all relative phases. Notice from Fig. 13 that, unlike the multiuser system in the presence of NEXT and FEXT, the performance in the presence of two NEXTs degrades when the relative phases for the two NEXTs are the same, i.e., $\phi_i = \varphi_i$, $i = 0, 1, \cdots, 5$. This is because the cross power spectrum $CPS(X_1, X_2)$ between the interferers having similar characteristics increases when their relative phases are the same, which results in a substantial decrease in the eigenvalue λ_2 of (18). The eigenvalue λ_2 with the optimum phase is about 3.6 times larger than that with the worst phase ($\overline{\lambda}_{2,optimum} = 1.1498 \times 10^{-4}$, $\overline{\lambda}_{2,worst} = 3.1940 \times 10^{-5}$), thus leading to 5.6 dB performance improvement for the optimum phase compared to the worst relative phase case, as shown in Fig. 13.

IV. CONCLUSIONS

We have discussed the cyclostationary crosstalk suppression in multiuser environment. The equalizer's eigenstructure in the presence of multiple cyclostationary interference has been analyzed, and its excess MSE and MMSE have been computed by using the eigenstructure. This theoretical analysis of the performance of interference suppression has been verified by computer simulation for multiuser wired communication system. In particular, it has been shown that the $2N(K+1)$ eigenvalues in the presence of K cyclostationary interferers are classified into $K+1$ different eigenvalue sets, i.e., λ_i, $i = 0, 1, \cdots, K$, and the convergence speed as well as the steady-state performance is determined by the smallest eigenvalue λ_K, which depends on the folded interferer power spectrum, the cross power spectrum between the signal and the interferer, and the cross power spectrum between the interferers. We have also shown that FEXT suppression is more difficult than NEXT suppression because of the large cross-correlation between the signal and the crosstalk for the FEXT case. Furthermore, with an idealized model and measured characteristics of NEXT/FEXT channel, the optimum and worst relative clock phases among the signal and multiple interferers have been obtained using the equalizer's eigenstructure. The optimum and worst relative phases vary depending on the characteristics of multiple interferers. Specifically, the performance in the presence of multiple interferers having similar characteristics degrades when the relative phases among multiple interferers are the same. Analysis and computer simulation results indicate that about 10 dB performance improvement and about 10 times faster convergence speed can be achieved by employing the optimum relative clock phase for multiuser wired communication system in the presence of NEXT and FEXT.

REFERENCES

[1] J. Salz, "Digital transmission over cross-coupled linear channels," *AT&T Tech. J.*, vol. 64, no. 6, pp. 1147–1157, July/Aug. 1985.

[2] J. J. Werner, "The HDSL environment," *IEEE J. Select. Areas Commun.*, vol. 9, no. 6, pp. 785–800, Aug. 1991.

[3] T. Starr, J. M. Cioffi, and P. J. Silverman, *Understanding Digital Subscriber Line Technology*, Prentice Hall, 1999.

[4] W. Y. Chen, *DSL Simulation Techniques and Standards Development for Digital Subscriber Line Systems*, Macmillan Technology Series, 1998.

[5] G. H. Im *et al.*, "51.84 Mb/s 16-CAP ATM LAN standard," *IEEE J. Select. Areas Commun.*, vol. 13, no. 4, pp. 620–632, May 1995.

[6] W. Y. Chen, G. H. Im, and J. J. Werner, "Design of digital carrierless AM/PM transceivers," AT&T/Bellcore Contribution T1E1.4/92–149, Aug. 19, 1992.

[7] B. Daneshrad and H. Samueli, "A 1.6 Mb/s digital-QAM system for DSL transmission," *IEEE J. Select. Areas Commun.*, vol. 13, no. 9, pp. 1600–1610, Dec. 1995.

8] D. D. Harman *et al.*, "Local distribution for IMTV," *IEEE Multimedia*, vol. 2, no. 3, pp. 14–23, Fall 1995.
9] N. R. Shanbhag and G. H. Im, "VLSI systems design of 51.84 Mb/s transceivers for ATM-LAN and broadband access," *IEEE Trans. Signal Processing*, vol. 46, no. 5, pp. 1403–1416, May 1998.
10] Special Issue on Very high-speed Digital Subscriber Lines, *IEEE Commun. Mag.*, vol. 38, no. 5, May 2000.
11] V. Oksman and J. J. Werner, "Single-carrier modulation technology for very high-speed digital subscriber line," *IEEE Commun. Mag.*, vol. 38, no. 5, pp. 82–89, May 2000.
12] G. H. Im, K. M. Kang, and C. J. Park, "FEXT cancellation for twisted-pair transmission," *IEEE J. Select. Areas Commun.*, vol. 20, no. 5, pp. 959–973, June 2002.
13] J. C. Campbell, A. J. Gibbs, and B. M. Smith, "The cyclostationary nature of crosstalk interference from digital signals in multipair cable- part I and II," *IEEE Trans. Commun.*, vol. 31, pp. 629–649, May 1983.
14] E. Biglieri, M. Elia, and L. Lopresti, "The optimal linear receiving filter for digital transmission over nonlinear channels," *IEEE Trans. Inform. Theory*, vol. 35, no. 3, pp. 620–625, May 1989.
15] B. R. Petersen and D. D. Falconer, "Minimum mean square equalization in cyclostationary and stationary interference-analysis and subscriber line calculations," *IEEE J. Select. Areas Commun.*, vol. 9, pp. 931–940, Aug. 1991.
16] M. L. Honig, P. Crespo, and K. Steiglitz, "Suppression of near- and far-end crosstalk by linear pre- and post-filtering," *IEEE J. Select. Areas Commun.*, vol. 10, no. 3, pp. 614–629, Apr. 1992.
17] W. A. Gardner, ed., *Cyclostationarity in Communications and Signal Processing*, New York: IEEE Press, 1994.
18] G. H. Im, H. C. Won, and C. J. Park, "Convergence behavior of a phase-splitting fractionally spaced equalizer in the presence of a cyclostationary crosstalk interference," *IEEE Commun. Lett.*, vol. 4, no. 8, pp. 261–263, Aug. 2000.
19] H. C. Won and G. H. Im, "Crosstalk equalization for high-speed digital transmission systems," *IEICE Trans. Commun.*, vol. E86-B, no.3, Mar. 2003.
20] G. H. Im and N. R. Shanbhag, "A pipelined adaptive NEXT canceller," *IEEE Trans. Signal Processing*, vol. 46, no. 8, pp. 2252–2258, Aug. 1998.
21] J. J. Werner, "An echo-cancellation-based 4800 bit/s full-duplex DDD modem," *IEEE J. Select. Areas Commun.*, vol. 2, no. 5, pp. 722–730, Sept. 1984.
22] G. H. Im, C. K. Un, and J. C. Lee, "Performance of a class of adaptive data-driven echo cancellers," *IEEE Trans. Commun.*, vol. 37, no. 12, pp. 1254–1263, Dec. 1989.
23] G. H. Im and K. M. Kang, "Performance of a hybrid decision feedback equalizer structure for CAP-based DSL systems," *IEEE Trans. Signal Processing*, vol. 49, no. 8, pp. 1768–1785, Aug. 2001.
24] R. D. Gitlin, J. F. Hayes, and S. B. Weinstein, *Data Communications Principles*, Plenum Press, 1992.
25] F. Ling and S. U. H. Qureshi, "Convergence and steady-state behavior of a phase-splitting fractionally spaced equalizer," *IEEE Trans. Commun.*, vol. 38, no. 4, pp. 418–425, Apr. 1990.
26] J. H. Wilkinson, *The Algebraic Eigenvalue Problem*, Clarendon, Oxford, 1965.

Gi-Hong Im received the B.S. degree in electronics engineering from Seoul National University (SNU), Seoul, in 1980, and M.S. and Ph.D. degrees in electrical engineering from Korea Advanced Institute of Science and Technology (KAIST), Seoul, in 1983 and 1987, respectively.

From 1990 to 1996, he was a Member of Technical Staff in the Advanced Multimedia Communications Department at AT&T Bell Laboratories, Holmdel, NJ, where he was responsible of design and implementation of high-speed digital transmission systems for loop plant, local area network and broadband access applications, such as ADSL, ATM-LAN, and FTTC/VDSL. He has authored or co-authored more than twenty standards contributions to standards organizations such as ANSI T1E1.4, ETSI, IEEE 802.9, ANSI X3T9.5, and the ATM Forum. These contributions have led to the adoption of three AT&T proposals for new standards for high-speed LANs and broadband access over UTP wiring. Since 1996, he has been with POSTECH as a professor. From 1996 to 1999, he was a Bell Laboratories Technical Consultant. From 2002 to 2003, he was a visiting vice president in i-Networking Lab at Samsung Electronics, where he worked on 4G wireless communication systems. His current research interests include signal processing and digital communications with applications to high-speed digital transmission systems.

Dr. Im received the 1996 Leonard G. Abraham Prize Paper Award for best paper from the IEEE Journal on Selected Areas in Communications, and the 2000 LG faculty award from LG Electronics, Co., Ltd., Korea. He holds five U.S. patents with seven more patents pending.

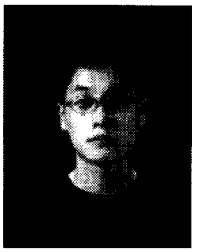

Hui-Chul Won received the B.S. and M.S. degrees in electronic and electrical engineering from Pohang University of Science and Technology (POSTECH), Kyungbuk, Korea, in 1998 and 2000, respectively. He is currently working toward the Ph.D. degree at Communications Research Lab., POSTECH. His current research interests are channel estimation methods, OFDM wireless communications systems, and high-speed digital transmission systems.